Conference Paper, Published Version

Tomiczek, Tori; Wargula, Anna; Jendrysik, Marie; Goodwin, S.; Kennedy, A. B.; Lynett, P.; Lomonaco, P.; Cox, D. T.

Physical Model Investigation of Parcel-Scale Effects of Mangroves on Wave Transformation and Force Reduction in the Built Environment

Coastal Structures 2019 - Nils Goseberg, Torsten Schlurmann (eds) - © 2019 Bundesanstalt für Wasserbau
ISBN 978-3-939230-64-9 (Online) - DOI: 10.18451/978-3-939230-64-9_100

Physical Model Investigation of Parcel-Scale Effects of Mangroves on Wave Transformation and Force Reduction in the Built Environment

T. Tomiczek, A. Wargula, M. Jendrysik & S. Goodwin
United States Naval Academy, Annapolis, USA
A.B. Kennedy
University of Notre Dame, Notre Dame, USA
P. Lynett
University of Southern California, Los Angeles, USA
P. Lomonaco, & D.T. Cox
Oregon State University, Corvallis, USA

Abstract: Coastal communities are challenged to develop sustainable adaptations to mitigate hazards associated with rising seas and intensifying storms. Based on field and laboratory studies, we quantified parcel-scale benefits of mangrove shorelines, building on observations of mangrove protection of near-shore residential infrastructure in the Florida Keys following Hurricane Irma (2017). We measured the trunk diameter, prop root diameter, prop root height, and elastic modulus of the *Rhizophora mangle* species to construct a 1:16 scale physical model of a mangrove trunk-prop root system. Hydraulic experiments were conducted in Oregon State University's Directional Wave Basin with an idealized shoreline comprised of a mangrove test section in front idealized structure to represent a coastal community. The experiment was designed to quantify the effects of varying cross-shore thicknesses of mangroves on the flow conditions and hydrodynamic loads on idealized structures. Preliminary results indicate that mangrove cross-shore thicknesses of 0.51 m (8.2 m full scale) reduced the force by 22-43% compared to that measured on an unshielded structure. Additional load reduction was observed when mangrove cross-shore thickness was increased to 1.19 m (19.0 m full scale). Further work is needed to quantify the benefits of natural and nature based features at different scales and in real systems, such as in conjunction with hardened coastal infrastructure.

Keywords: natural and nature based features; mangroves; wave loads on structures

1 Introduction

Coastal communities today face increasing challenges due to rising seas and storms of increasing intensity. In the United States alone, the 2017 and 2018 Atlantic hurricane seasons account for five of the top 20 costliest weather and climate-related disasters in U.S. history, with Hurricanes Harvey, Maria, and Irma (2017) ranking second, third, and fifth, respectively (NOAA, 2019). Therefore, coastal engineers, land use managers, stakeholders, and residents must work together to develop sustainable, resilient solutions that allow communities to adapt to changing coastal conditions and continue to thrive.

In recent years, natural and nature based features including coastal wetlands and mangroves have received attention as viable shoreline protection solutions due to their wave mitigation, flood storage capacity, and ecological, social, and cultural co-benefits (Reid et al., 2005; Farber et al., 2006; Scyphers et al., 2011; 2015; Narayan et al., 2016). In particular, mangroves have been noted to protect property and human life during previous tsunami (Giri et al., 2011; Kathiresan and Rajendran, 2005; Alongi, 2008) and storm surge events (Zhang et al., 2012; Guannel et al., 2016). Specifically, we refer to the *Rhizophora* mangrove species, characterized by their complex system of above-ground prop roots, also called stilt roots, which obstruct flow and dissipate energy during elevated wave and storm surge conditions. Many observations of avoided or reduced damage have been recorded for large (km) scale mangrove forests. Recently, however, Tomiczek et al. (2019) observed similar wave and surge damage mitigation to residential structures in Key West and Big Pine Key, FL, located behind patchy,

parcel scale (10 to 100 m) mangrove fringes during Hurricane Irma. The authors noted reduced damage states experienced by structures located behind these mangrove fringes compared to those located behind sandy beaches, revetments, and seawalls subject to similar hindcast hydrodynamic conditions.

A number of laboratory, field, and computational investigations have measured or calculated wave and velocity attenuation through mangrove trunk-prop root systems or quantified drag coefficients on mangrove specimens (Mazda et al., 1997; Hashim and Catherine, 2013; Liu, et al., 2015; Horstman et al., 2014; Zhang et al., 2015; Tinoco and Coco, 2016; Chang et al., 2017; Ismail et al., 2017; Maza et al., 2017; Kazemi et al., 2018; Tinoco and Coco, 2018). For example, Horstman et al. (2014) performed field measurements in Thailand to measure wave attenuation and sedimentation rates, observing that mangroves both reduced wave energy and facilitated net sediment deposition rates along the sample transects. Zhang et al. (2012) evaluated field observations and numerical results of storm surge inundation in South Florida due to Hurricane Wilma (2005) and found that while storm surge levels tended to increase seaward of the mangrove zone, the surge amplitude and inland extent were significantly decreased by the 6-30 km wide mangrove forests. Zhang et al. (2015) constructed a 1:7.5 scale model of a mangrove forest to measure mean flow velocities, Reynolds stress, and turbulent kinetic energy around stilt roots. Based on the detailed methodology for *Rhizophora* parameterization developed by Ohira et al. (2013), Maza et al., (2017) constructed a 1:12 scale model of a mature *Rhizophora* mangrove forest and measured the drag force on individual trees and water velocities around stilt roots. The authors found that velocities were reduced by up to 50% within the root zone compared to upstream conditions. Kazemi et al. (2018) used particle image velocimetry (PIV) to investigate the hydrodynamics of mangrove roots using a simplified array of cylinders.

While these and other studies have made progress towards characterizing the engineering performance of mangrove systems for coastal protection, questions remain about the potential of these systems to function during extreme events and the scale at which sufficient protection can be attained. Performance of parcel scale, patchy mangrove fringes similar to those seen in the Florida Keys and other developed subtropical locations is required to understand the protection provided for future mitigation and adaptation planning. In addition, while previous studies have focused on wave interaction with *Rhizophora*, little is known about the effects of these systems on inland wave-structure interaction.

This study investigates the effects of a mangroves fringe's cross-shore thickness on inland hydrodynamic characteristics and pressures and forces on idealized coastal structures for both tsunami-like and irregular wave conditions using a 1:16 scale physical model. The model was developed based on field measurements of mangrove geometric characteristics from Key West, FL, as well as the parameterization presented by Ohira et al. (2013). Pressures and loads on idealized structural elements positioned in a coastal urban array were measured in the presence of two configurations of mangroves with varying cross-shore thickness, as well as for waves interacting with the structures unshielded by mangroves. In the following sections, we describe the field characterization and parameterization of the mangrove model (Section 2), the laboratory setup, wave conditions, and instrumentation used for experimental configurations tested at Oregon State University's Directional Wave Basin (DWB) (Section 3), and results of hydrodynamic parameters and loads recorded on and around structures with and without shielding by the mangrove models (Section 4). Section 5 discusses implications of these experiments and points toward future and ongoing work to fully understand the capabilities of these systems as a nature-based engineering solution, as well as conclusions of this work.

2 Field Measurements and Scaling of Rhizophora Mangle

2.1 Field Measurements in Key West, Florida

Small-scale field experiments were conducted in July, 2018 to measure geometric characteristics of *Rhizophora mangle* in Key West, Florida. Seven sites were evaluated around the island with mangrove fringes with cross-shore expanses ranging from 30 - 250m. Sites were evaluated to determine the number of trees, trunk diameter, prop root diameter, number of prop roots in one square meter, average elevation at which prop roots extended from the main trunk, and average elastic modulus of prop roots. Figure 1 shows field measurements of prop root diameters (Fig. 1a) and a

histogram showing the distribution of prop root diameters across all of the test sites (Fig. 1b). Prop root diameters were binned by 0.005 m increments ranging from 0.000 - 0.070 m. As shown in Fig. 1b, the histogram of prop root diameters is bimodal with a left skew, indicating that a majority of measured roots were between 0.015 - 0.025 m. A second peak of larger root diameters (0.030 - 0.040 m) were observed; these larger diameters were typically observed at sites on the southern coast of Key West that were exposed to the Atlantic Ocean rather than the sheltered northern coast.

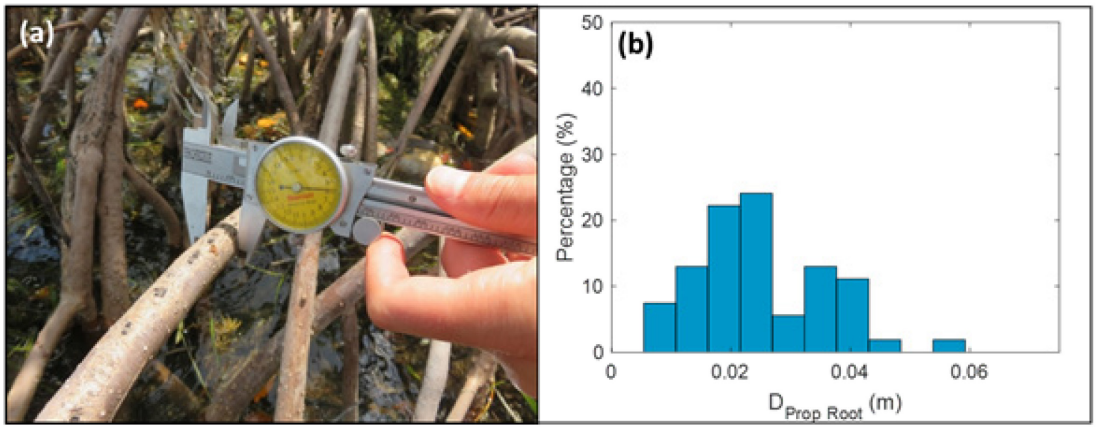

Fig. 1. (a) Prop root diameter measurements in Key West, FL; (b) Histogram showing distribution of prop root diameters measured during field study.

2.2 Literature Parametrizations and Scaling of Rhizophora Trunk-Prop Root Systems

In addition to field measurements, reported values for typical mangrove geometries and parameterization informed model construction. Ohira et al. (2013) conducted extensive field work and presented equations to determine prop root diameters, elevations at which prop roots connected to the mangrove trunk, and horizontal distance between the trunk and prop root terminus. Based on this parameterization, Maza et al. (2017) constructed a 1:12 scale model to estimate drag force coefficients and water velocities within a *Rhizophora* mangrove forest. Zhang et al. (2015) similarly constructed a large scale physical prop root model based on field measurements of prop root geometry and elasticity, reporting prop root porosities of 0.96-0.98 and a Young's Modulus of 15 GPa.

Based on these studies, we constructed 100 physical models of a *Rhizophora mangle* trunk-prop root system on a 1:16 geometric scale. Trunks were constructed of 1.3 cm diameter PVC rod, with 11 holes drilled into the trunk in a spiral pattern. Holes were spaced at 1.3 cm vertically, ranging from 2.5 – 15.2 cm above the base of the trunk, with 45° rotation between subsequent holes. Galvanized steel wire with a 2.5 mm nominal diameter was used for the roots; roots extended from either side of the PVC rod, creating a total of 22 roots on each mangrove.

3 Laboratory Measurements of Hydrodynamic Conditions, Pressures and Loads with and without Mangroves

3.1 Laboratory Setup and Wave Conditions

Physical model experiments were carried out at Oregon State University's DWB. Within the 48.8 m x 26.5 m plan dimensions of the basin, a 30 m long x 10 m wide test section concrete bathymetry was constructed; a plan and profile view of the test section can be seen in Fig. 2a and 2b, respectively. Waves generated by the wave maker propagated along a flat bathymetry for 11.7 m before reaching the onset of the test section, which comprised a 20 m long, 1:20 concrete slope followed by a 10 m x 10 m horizontal platform representing a bathymetry similar to that of a barrier island, from which water dropped into a 1 m deep recirculating basin. 100 idealized structural elements representing a coastal urban array were positioned on the barrier island bathymetry; each structure had dimensions 40 cm x 40 cm x 40 cm. Structures were spaced 0.6 m and 0.4 m apart (nearest edge to nearest edge) in the alongshore and cross-shore directions, respectively, with the first line of structures 1.6 m inland of the onset of the horizontal platform. Eight specimens were constructed of aluminum and

instrumented with pressure sensors, in-line load cells, and a six degree of freedom load cell as indicated in Fig. 2a, while the remaining specimens acting as macro roughness elements were constructed of concrete cinderblocks.

These experiments were part of a larger experimental campaign investigating the effects of macroroughness, seawalls, debris, and vegetation; this study focuses on configurations including mangrove vegetation and urban macroroughness elements. Three configurations were tested: zero rows of mangroves (M0), four rows of mangroves (M4), and eight rows of mangroves (M8). Rows were staggered, with trunk to trunk cross-shore distances of 0, 0.51 m, and 1.19 m, respectively, representing full-scale trunk to trunk cross-shore thicknesses of 0, 8.2, and 19.0 m, respectively. The alongshore expanse of the mangrove test section was 2.28 m, or 36.5 m at full-scale, representing the parcel-scale shoreline variation observed in the Florida Keys by Tomiczek et al. (2019). Mangroves were spaced according to trunk-density reports by Danielsen et al. (2005) and Clough et al. (1999), as well as technical guidance for mangrove restoration (EAD, 2015), with 0.17 m model cross-shore spacing and 0.19 m model alongshore spacing, resulting in a trunk density of 43 trees/m^2 (model-scale) or 17 trees/100 m^2 (full-scale). In all configurations with mangroves, the distance from the inland-most mangrove trunk to the first row of structures in the idealized urban array was 0.45 m. For the M8 configuration, the mangroves extended seaward to the onset of the 1:20 slope. Figure 3a and 3b shows photographs of the M4 and M8 configurations.

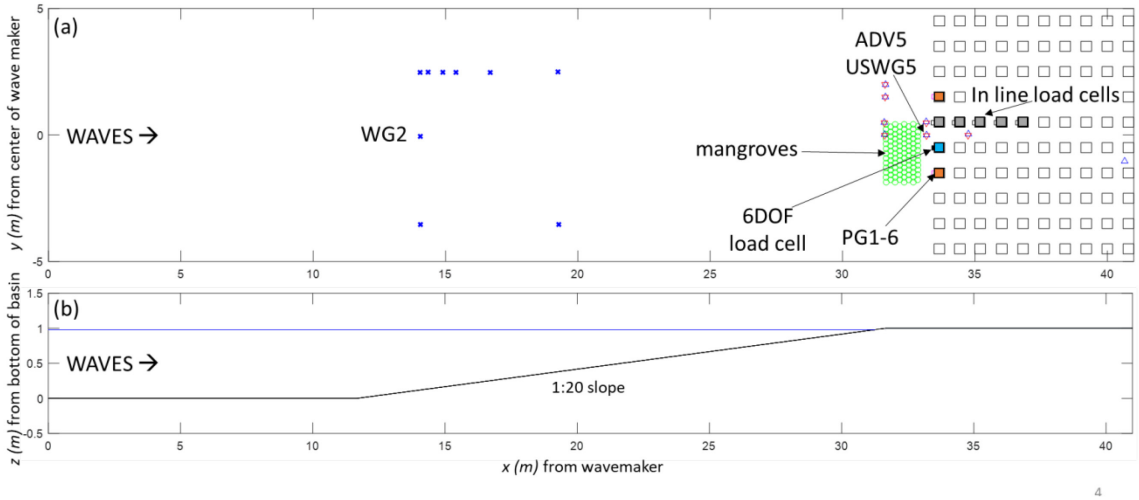

Fig. 2. (a) Plan; and (b) Profile view of the experimental test section, indicating positions of mangroves (shown: configuration M8) and instrumentation (wire resistance wave gauges (WGs) (blue exes); ADVs (blue triangles), ultrasonic wave gauges (USWGs) (red diamonds)). Also indicated are idealized structures instrumented with pressure sensors, in-line load cells, and a 6 degree-of-freedom load cell.

The DWB is equipped with a snake-type wave maker system with 30 independently-programmable servomotor-driven points and 29 paddles. Each board is 2.0 m high and has a maximum stroke of 2.1 m. A number of wave and flow conditions and water depths were simulated during experiments, including regular, random, solitary, and tsunami-like waves propagating with and without a background current. For this work we focus on tsunami-like waves with no background current. Waves were generated using an error function to create long period waves (e.g. Thomas and Cox, 2011). Table 1 lists the mean amplitude and representative period (calculated as the time during which the water surface elevation exceeded 10% of the wave amplitude) and standard deviations (in parentheses in Table 1) across all trials of the three wave conditions tested for each experimental configuration. Wave amplitudes and representative periods were recorded at a wire resistance wave gauge located at the onset of the test section's 1:20 bathymetric slope (WG2). As indicated by Table 1, offshore wave amplitudes were generally within one centimeter across all trials, and representative periods were within 0.01 - 0.15 s, with larger variation observed for the longest wave trial (ERF3).

Tab. 1. Experimental Wave Conditions (subset for this analysis)

Trial	$\bar{A}$ (m)	$\overline{T_R}$ (s)
ERF1	0.126 (0.009)	11.15 (0.14)
ERF2	0.144 (0.012)	8.30 (0.01)
ERF3	0.211 (0.009)	5.71 (0.03)

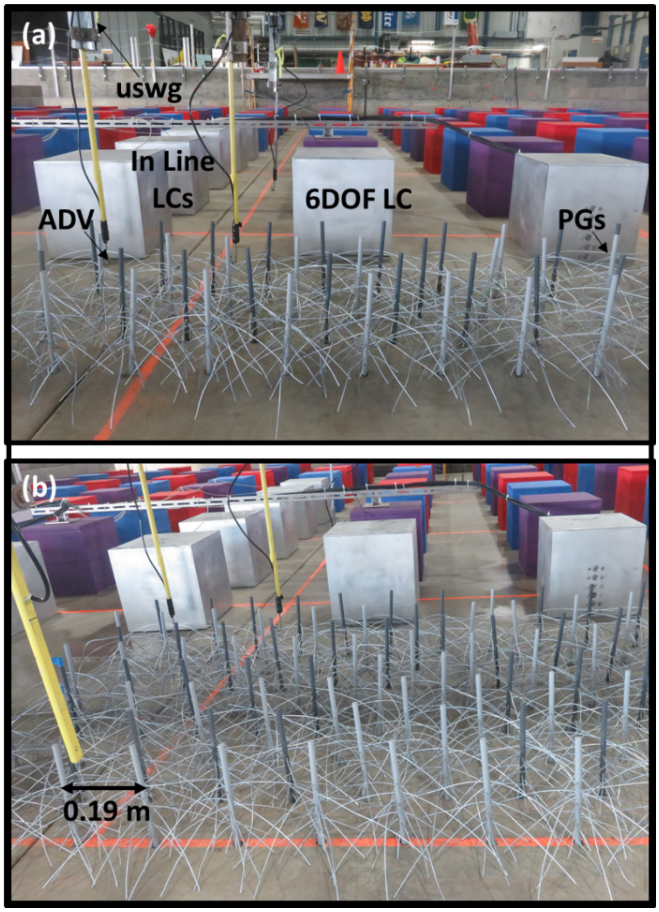

Fig. 3. Mangrove Configurations. (a) M4 (four rows of mangroves); and (b) M8 (eight rows of mangroves).

3.2 Instrumentation

As shown in Fig. 2(a), instrumentation including ultrasonic wave gauges (USWGs), wire-resistance wave gauges (WGs), acoustic Doppler velocimeters (ADVs), pressure gauges, in-line load cells, and a six degree of freedom load cell were positioned along the test section and on idealized structural elements to record water surface elevations, water velocities, pressures on idealized structures, and *x*-direction and six-degree of freedom loads felt by idealized structures, respectively. All instrumentation were synchronized, with wave gauges and ADVs recording at 100 Hz and pressure gauges and load cells recording at 1000 Hz. For varying offshore wave conditions, this study focuses on the effects of each mangrove configuration on water surface elevations and velocities measured directly behind mangroves (USWG5 and ADV5, respectively) and on cross-shore loads sustained by a specimen instrumented with a six-degree-of freedom load cell positioned directly behind mangrove rows. The *x, y,* and *z* positions of each of instrument discussed in this paper are listed in Table 2, referenced to the DWB coordinate system, a right–handed coordinate system where the *x*-axis is the cross-shore coordinate (m), positive onshore; the *z*-axis is the vertical coordinate (m), positive upwards; and the *y*-axis is the alongshore coordinate (m), its origin at the alongshore centerline of the tank and positive to the left when facing onshore.

Tab. 2. Selected Instrumentation Locations

Instrument	*x (m)*	*y (m)*	*z (m)*
Wave maker center	0.00	0.00	0.00
WG2	14.048	-0.056	--
USWG5	33.17	-0.003	2.357
ADV5	33.17	-0.026	1.018
6DOF Load cell (F_x)	33.46	-0.511	1.083

4 Mangrove Effects on Inland Water Surface Transformation, Velocities, and Loads

4.1 Effects on Water Surface Transformation

Figure 4a-c shows the time series of water surface elevations measured at USWG5, positioned 0.1 m seaward of the leading edge of the urban array and 1.5 m inland of the onset of the horizontal platform for the M0 (black lines), M4 (blue dashed lines), and M8 (red dash-dot) mangrove configurations for trials ERF1, ERF2, and ERF3, respectively. The presence of mangroves increased the water surface elevation behind the mangroves, with peak water surface elevations amplified by a factor of 1.6 - 2.0 compared to the configurations with only urban roughness elements. We hypothesize that this amplification of the water surface was due to wave interaction with the mangrove trunks and root system due to splash up and changes to wave breaking dynamics associated with the added roughness elements. Additionally, reflection from mangroves and structures likely caused damming and increased water surface elevations between mangroves and structures. Compared to the difference between the M0 and M4 configurations, the differences in water surface elevations for the M4 and M8 configurations were small for wave trials considered here, with the peak water surface elevations within 12%.

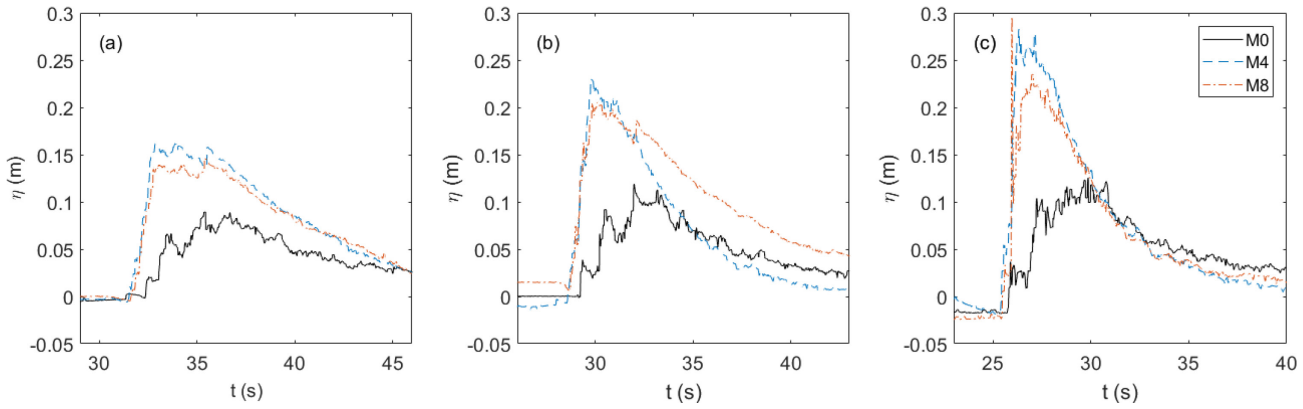

Fig. 4. Water surface elevation time series for M0 (black lines), M4 (blue dashed lines), and M8 (red dash-dot lines) configurations: (a) ERF1, $\bar{A}$=0.126 m, $\overline{T_R}$= 11.15 s; (b) ERF2, $\bar{A}$=0.144 m, $\overline{T_R}$= 8.30 s; (c) ERF3, $\bar{A}$=0.211 m, $\overline{T_R}$= 5.71 s.

4.2 Effects on Cross-Shore Velocities

Figure 5a-c shows the time series of cross-shore water velocities u measured at the ADV positioned 0.1 m seaward of the leading edge of the urban array and 1.5 m inland of onset of the horizontal platform for the M0 (black lines), M4 (blue dashed lines), and M8 (red dash-dot) mangrove configurations for trials ERF1, ERF2, and ERF3, respectively. Velocity measurements suggest that wave breaking was triggered earlier in trials with mangroves, compared to the no mangroves case (blue and red scatter (M4 and M8) occurs earlier than black scatter (M0) in Fig. 5). To quantify the effects of mangrove configurations on velocity, the upper third of the onshore-directed (positive) velocity magnitude after breaking (defined as the scatter in Fig. 5) was averaged for each trial and compared. For the lowest-velocity wave, ERF1 (Fig. 5a), there was little difference in the velocity magnitude (7% and 2% decrease for M4 and M8, respectively, compared to M0). ERF2 velocities (Fig. 5b) decreased by 59% and 53%, while ERF3 velocities (Fig. 5c) decreased by 47% and 50% from M0 to M4 and M8, respectively. Although the presence of mangroves affected the timing and cross-shore position of breaking and the magnitude of the cross-shore velocities, the cross-shore thickness of the mangroves did not significantly impact the change in cross-shore velocity. The degree of increase or decrease in the water velocity due to the mangroves changed for varying wave conditions (amplitude and representative period), which may be due to the change in drag on the mangroves and the change in location of wave breaking, as well as potential damming effects between the mangroves and urban array.

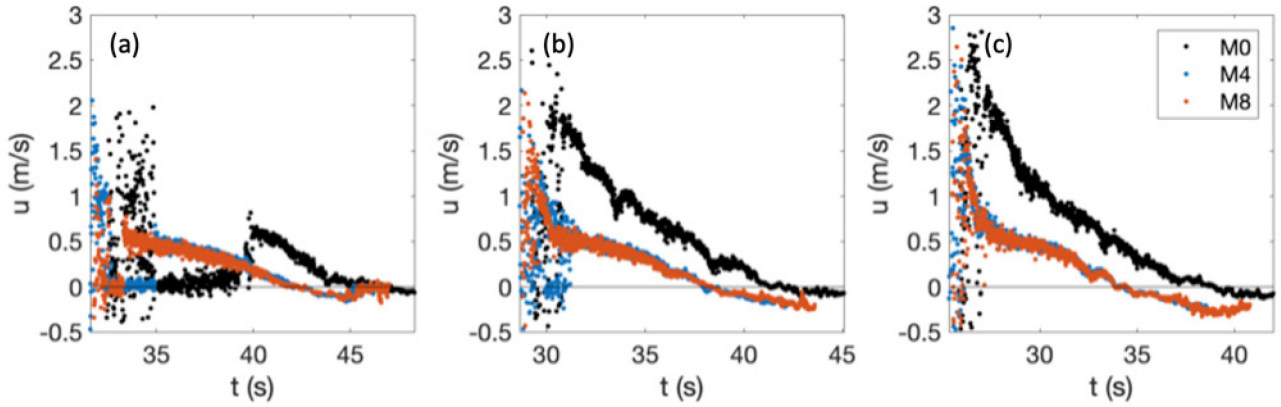

Fig. 5. Cross-shore water surface velocity series at ADV located behind M0 (black points), M4 (blue points), and M8 (red points) configurations: (a) ERF1, $\bar{A}$=0.126 m, $\overline{T_R}$= 11.15 s; (b) ERF2, $\bar{A}$=0.144 m, $\overline{T_R}$= 8.30 s; (c) ERF3, $\bar{A}$=0.211 m, $\overline{T_R}$= 5.71 s. Large scatter in the data was retained to show wave breaking.

4.3 Effects on Cross-Shore Loading

Figure 6a-c shows the time series of loads measured by a six-degree of freedom load cell installed in a specimen positioned 0.41 m behind the inland-most line of mangroves (structure edge to trunk center), or 1.60 m from the onset of the horizontal platform for ERF1, ERF2, and ERF3. Only cross-shore effects were considered here; therefore, the loads plotted in Fig. 6 represent loads recorded in the *x*-direction (in the direction of wave propagation). Colors indicate the degree of shielding, with black lines, blue dashed lines, and red dash-dot lines indicating the M0, M4, and M8 cases, respectively.

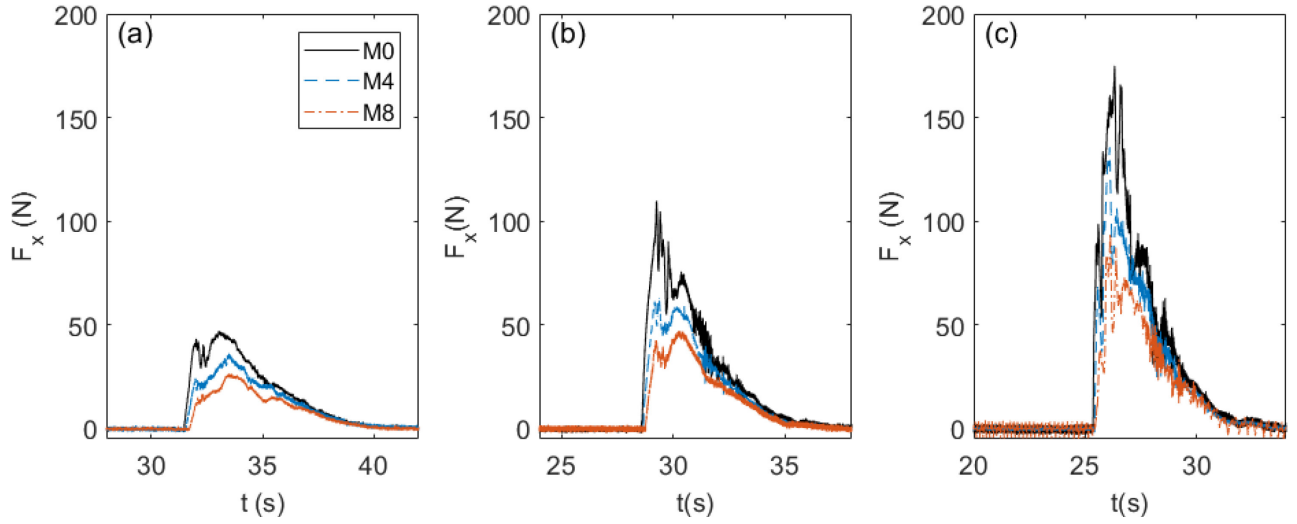

Fig. 6. Cross-shore load time series (F_x) measured by six-degree of freedom load cell on specimen 1.60 m inland of onset of horizontal platform for M0 (black lines), M4 (blue dashed lines), and M8 (red dash-dot lines) configurations: (a) ERF1, $\bar{A}$=0.126 m, $\overline{T_R}$= 11.15 s; (b) ERF2, $\bar{A}$=0.144 m, $\overline{T_R}$= 8.30 s; (c) ERF3, $\bar{A}$=0.211 m, $\overline{T_R}$= 5.71 s.

As seen in Fig. 6, waves with shorter periods and larger amplitudes (ERF3) caused the largest forces on the specimen, with increasing cross-shore thicknesses of fronting mangroves providing reductions in the total measured force. Figure 7a plots the peak wave force F_x measured against the cross-shore distance of the shielding mangrove fringe (measured trunk to trunk) for each wave condition tested: ERF1 (black circles), ERF2 (blue upward triangles), and ERF3 (red squares). Figure 7a confirms that the peak force experienced by the instrumented specimen decreased with increasing mangrove cross-shore thicknesses.

Figure 7b normalizes the data shown in Fig. 7a by plotting the percent reduction in force compared to the unshielded case, calculated as $(F_x(unshielded)-F_x(shielded))/F_x(unshielded)$, against the cross-shore thickness of mangroves $X_{mangrove}$ between the onset of the horizontal test section and the leading edge of the first row of structures. Similar to Fig. 7a, black circles, blue upward triangles, and red

squares indicate ERF1, ERF2, and ERF3, respectively. In general, a larger percent reduction is observed between the M0 and M4 configurations, when four rows of mangroves were added to the test bathymetry. While the force on the specimen was further reduced between the M4 and M8 configurations, the differences between the M4 and M8 configurations were less significant than between M0 and M4 configurations. For example, the force in the *x*- direction was reduced by 23% for ERF1 when four rows of mangroves (0.51 m cross-shore thickness, 8.16 m full scale) were added to the baseline M0 configuration; installing an additional 4 rows (1.19 m cross-shore thickness, 19.04 m full scale) induced a further reduction in load by 21%. The percent reduction recorded for the M4 configuration compared to the M0 configuration for the ERF2 and ERF3 trials were 43% and 22%, while the additional reduction in the M8 configurations were 14% and 24%, respectively. Therefore, significant shoreline protection may be provided by mangrove shorelines in the first few meters of the mangrove fringe. Under certain wave conditions, further increasing the mangrove cross-shore thickness may provide additional force reduction on inland structure.

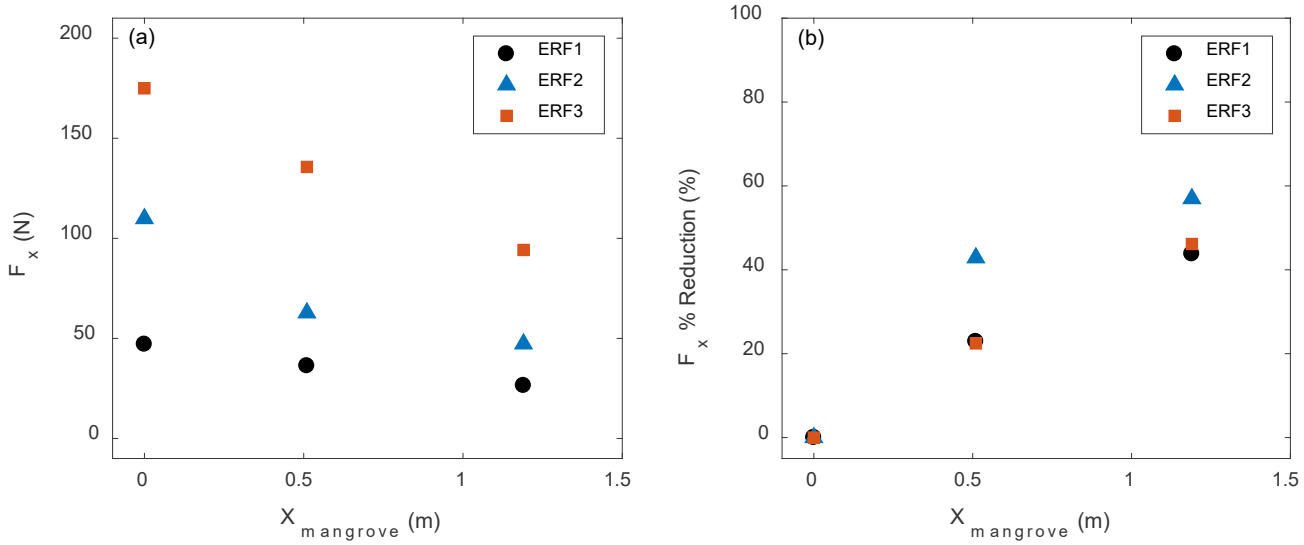

Fig. 7. (a) Peak cross-shore force (F_x) measured by six-degree of freedom load cell on specimen vs. cross-shore thickness of shielding mangrove fringe ($X_{mangrove}$) for ERF1 (black circles), ERF2 (blue upward triangles), and ERF3 (red squares); (b) Percent reduction in cross-shore force on specimen (%) vs. cross-shore thickness of mangrove fringe ($X_{mangrove}$) for ERF1 (black circles), ERF2 (blue upward triangles), and ERF3 (red squares).

5 Discussion and Conclusions

The data presented above corroborate previous observations that mangroves and other natural and nature based features may dissipate wave energy and reduce the cross-shore force on near coast structures shielded by these systems. While other works have recorded wave attenuation by mangrove fringes, the water surface amplification observed in these trials is likely due wave breaking processes associated with the additional roughness created by the mangrove fringe, as well as reflection due to the urban array and mangroves. These higher water surface elevations were coupled with reduced cross-shore water velocities and forces measured on an instrumented specimen located inland of the mangroves, which may be partially due to relationships between momentum flux and the total force on a structure.

We make the following conclusions from this analysis:

- The presence of mangroves changed the hydrodynamics of waves in front of the urban array. Water surface elevations generally increased when four or eight rows of mangroves were added to the test section. Peak velocities tended to decrease for short period waves (high velocities, ERF2/ERF3) and increase for the long period wave (low velocities, ERF1) behind the mangroves. These changes to hydrodynamics may be due to the change in wave breaking location and added turbulence as flow propagated through the mangrove fringe.

- The presence of mangroves significantly reduced the load measured on an idealized structure. Load reductions between 22-57% were recorded for when the structure was shielded by four to eight rows of mangroves compared to unshielded conditions.
- Despite significant differences observed between M0 and M4 configurations, installing additional cross-shore thickness of mangroves did not significantly affect water surface elevations or velocities. While forces measured for the M8 configuration were reduced, for the ERF1 and ERF2 conditions the reduction was similarly less than that between the M0 and M4 configurations. Additional work is needed to quantify physical processes inducing energy dissipation due to flow propagation through and around root-trunk systems of *Rhizophora* species and to identify required cross-shore thicknesses for effective and efficient shoreline protection.

While these data show that natural and nature based features can provide protection at the parcel scale, several important considerations must be explored in future work. First of all, scaling effects must be evaluated to ensure that the physical model is not affected by phenomena not expected at prototype scales. For example, the Reynolds Number must be sufficiently large to ensure that viscous effects do not dominate the inertial effects typical of overland flow. With water velocities for mangrove trails between 0.5 - 1.5 m/s, the Reynolds Number for flow around mangrove roots ranged from 1200-3700, sufficient to generate turbulent wakes (Maza et al., 2017). Additional work is required to identify and quantify the onset of turbulence generated by individual roots and root systems for mangrove-flow interaction. Tests at additional geometric scales will better resolve scale effects for application at prototype scales.

In addition, a wider variety of mangrove configurations may be tested in future work. Mangroves in nature grow at irregular positions with random arrays of roots. Additional randomization in laboratory setup will allow for parameterization and generalization of mangrove benefits at sparser or denser spacing than those considered in these trials. Furthermore, the wave conditions presented here represent long waves; however, there are still significant differences in period when scaling laboratory conditions to those of a tsunami. Therefore, the performance and effects of mangrove fringes both for longer period tsunami-like waves as well for shorter period waves such as hurricane waves and storm surge must be further quantified. These short-period, random wave conditions were tested during laboratory experiments and are the subject of ongoing work.

Finally, the performance of mangroves in real systems must be better understood, both for natural mangrove fringes and when coupled with engineering structures such as seawalls and revetments as part of a hybrid solution. Additional field measurements can quantify the interaction of mangroves with these structures and the performance of hybrid systems in attenuating waves and water velocities during daily extreme conditions. Better understanding these hybrid systems may allow for strategic coastal planning to improve the resiliency of coastal communities worldwide.

6 Acknowledgements

The authors gratefully acknowledge the expertise and leadership of Louise Wallendorf, Bill Beaver, and Brandon Stanley, who were instrumental in model construction and preliminary testing at the United States Naval Academy. Dr. Michael Johnson, Dr. Hyoungsu Park, Adam Keen, Joaquin Pablo Moris Barra, Kiera O'Donnell, Tim Maddux, and Morgan Wade were also instrumental contributors during either field or laboratory experiments. This project was funded by the National Science Foundation CMMI Grant #s1825080, 1661015, 1661052, and 166131, NHERI (National Science Foundation CMMI Grant #1519679, and the U.S. Army Corps Engineers' Engineering Research and Development Center. Any opinions, findings, and conclusions or recommendations expressed in this material are those of the authors and do not necessarily reflect the views of the U.S. Army Corps of Engineers, National Science Foundation, or United States Naval Academy. The experimental data are available by contacting the first authors.

References

Alongi, D.M., 2008. Mangrove forests: resilience, protection from tsunamis and responses to global climate change. Estuarine, Coastal and Shelf Science, 76 (1), 1-13.

C. Chang, Liu, P. L-F., Mei C.C., and Maza, M. 2017. Periodic water waves through a heterogeneous coastal forest of arbitrary shape. 122, 2017, 141-157

Clough, B.F., Tan, D.T., Buu, D.C., Phuong, D.X., 1999. Mangrove forest structure and growth. In: Clough, B.F. (Ed.), Mixed Shrimp Farming- Mangrove Forestry Models in the Mekong Delta, Termination Report, Part B: Technical Appendices. Australian Centre for International Agricultural Research, Canberra, pp. 235-251.

Danielsen, F., Serensen, M.K., Olwig, M.F., Selvam, V., Parish, F., Burgess, N.D., Hiraishi, T., Karunagaran, V.M., Rasmussen, M.S., Hansen, L.B., Quarto, A., and Suryadiputra, N. 2005. The Asian tsunami: A protective role for coastal vegetation: Supporting Online Material. Science, 310 (5748), 643. DOI: 10.1126/science.1118387.

Environment Agency – Abu Dhabi (EAD). 2015. Technical Guidance Document for Mangrove Planting Permitting and Mangrove Plan. EAD-TBMS-TG-01. 44 pp.

Farber, S., Costanza, R., Childers, D.L., Erickson, J., Gross, K., Grove, M., Hopkinson, C.S., Kahn, J., Pincetl, S., Warren, A.T.P., Wilson, M., 2006. Linking ecology and economics for ecosystems management. BioScience, 56 (2), 121-133.

Giri, C., Long, J., Tieszen, L., 2011. Mapping and monitoring Louisiana's mangroves in the aftermath of the 2010 Gulf of Mexico oil spill. Journal of Coastal Research, 27 (6), 1059-1064.

Guannel, G., Arkema, K., Ruggiero, P., Verutes, G., 2016. The power of three: coral reefs, seagrasses and mangroves protect coastal regions and increase their resilience. PLoS ONE, 11 (7), e0158094.

Hashim, A.M., Catherine, S.M.P., 2013. A laboratory study on wave reduction by mangrove forests. APCBEE Procedia, 5, 27-32.

Horstman, E.M., Dohmen-Janssen, C.M., Narra, P.M.F., van den Berg, N.J.F., Siemerink, M., Hulscher, S.J.M.H., 2014. Wave attenuation in mangroves: a quantitative approach to field observations. Coastal Engineering, 94, 47-62.

Ismail, I., Husain, M.L., Zakaria, R., 2017. Attenuation of boat wakes in mixed mangrove forest of rhizophora and bruguiera species in Matang Perak. Malaysian Journal of Geosciences, 1 (2), 29-32.

Kathiresan, K., Rajendran, N., 2005. Coastal mangrove forests mitigated tsunami. Estuarine, Coastal and Shelf Science, 65 (3), 601-606.

Kazemi, A., Van de Riet, K., Curet, O.M., 2018. Drag coefficient and flow structure downstream of mangrove root-type models through PIV and direct force measurements. Physical Review Fluids,

Liu, P. L-F, Chang, C-W, Mei, C.C., Lomonaco, P., Martin, F.L., Maza, M. 2015. Periodic water waves through an aquatic forest. Coastal Engineering, 96, 2015, 100-117. doi:10.1016/j.coastaleng.2014.11.002

Maza, M., Adler, K., Ramos, D., Mikhail Garcia, A., Nepf, H., 2017. Velocity and drag evolution from the leading edge of a model mangrove forest. Journal of Geophysical Research: Oceans, 122, 9144-9159.

Mazda, Y., Wolanski, E., King, B., Sase, A., Ohtsuka, D., Magi, M., 1997. Drag force due to vegetation in mangrove swamps. Mangroves and Salt Marshes, 1 (3), 193-199.

Narayan, S., Beck, M.W., Reguero, B.G., Losada, I.J., van Wesenbeeck, B., Pontee, N., Sanchirico, J.N., Ingram, J.C, Lange, G.M., and Burks-Copes, K.A. 2016. The effectiveness, costs, and coastal protection benefits of natural and nature-based defences. PLoSONE, 11, 5, 17 pp.

NOAA National Centers for Environmental Information (NCEI) U.S. Billion-Dollar Weather and Climate Disasters 2019. https://www.ncdc.noaa.gov/billions/

Ohira, W., Honda, K., Nagai, M., Ratanasuwan, A., 2013. Mangrove stilt root morphology modeling for estimating hydraulic drag in tsunami inundation simulation. Trees, 27 (1), 141-148.

Reid, W.V., Mooney, H.A., Cropper, A., Capistrano, D., Carpenter, S.R., Chopra, K., Dasgupta, P., Dietz, T., Duraiappah, A.K., Hassan, R., Kasperson, R., Leemans, R., May, R.M., McMichael, T., Pingali, P., Samper, C., Scholes, R., Watson, R.T., Zakri, A.H., Shidong, Z., Ash, N.J., Bennett, E., Kumar, P., Lee, M.J., Raudsepp-Hearne, C., Simons, H., Thonell, J., and Zurek, M.B. 2005. Ecosystems and human well-being: Synthesis. Island Press, Washington, D.C.

Scyphers, S.B., Powers, S.P., Heck, K.L., Byron, D., 2011. Oyster reefs as natural breakwaters mitigate shoreline loss and facilitate fisheries. PloS ONE, 6 (8), e22396.

Scyphers, S.B., Gouhier, T.C., Grabowski, J.H., Beck, M.W., Mareska, J., Powers, S.P., 2015. Natural shorelines promote the stability of fish communities in an urbanized coastal system. PLoS ONE, 10 (6), e0118580.

Tinoco, R.O. and Coco, G. 2016. A laboratory study on sediment resuspension within arrays of rigid cylinders. Advances in Water Resources, 92, 2016, 1-9.

Tinoco R.O. and Coco, G. 2018 Turbulence as the Main Driver of Resuspension in Oscillatory Flow Through Vegetation. JGR Earth Surface, 123, 5, 891-904.

Tomiczek, Tori, Furman, K., Webbmartin, B., O'Donnell, K., and Scyphers, S. 2019. Community Resilience, Shoreline and Structural Vulnerabilities to Hurricane Irma in the Florida Keys. *Natural Hazards Review*, Revisions Submitted.

Thomas, S. and Cox, D. 2011. Influence of finite-length seawalls for tsunami loading on coastal structures. Journal of Waterway, Port, Coastal, and Ocean Engineering, 138(3), 203–214.

Zhang, K., Liu, H., Li, Y., Xu, H., Shen, J., Rhome, J., Smith, T.J., 2012. The role of mangroves in attenuating storm surges. Estuarine, Coastal and Shelf Science, 102-103 (1), 11-23.

Zhang, X., Chua, V.P., Cheong, H.-F., 2015. Hydrodynamics in mangrove prop roots and their physical properties. Journal of Hydro-environmental Research, 9 (2), 281-294.